Available online at www.sciencedirect.com
SCIENCE DIRECT
Talanta 68 (2006) 819–830
Talanta
www.elsevier.com/locate/talanta

Interpretation of non–Nernstian slopes in graphic analysis of data collected in pH range close to deprotonation of a ligand Part I. A glass electrode potentiometric and polarographic study of Cd–$(TAPSO)_x$–$(OH)_y$ and Zn–$(TAPSO)_x$–$(OH)_y$ systems

Carina M.M. Machado [a], Ignacy Cukrowski [b,1], Helena M.V.M. Soares [a,*]

[a] *REQUIMTE, Department of Chemical Engineering, Faculty of Engineering, University of Porto, Rua Dr. Roberto Frias, 4200-465 Porto, Portugal*
[b] *Department of Chemistry, University of Pretoria, Pretoria 0002, South Africa*

Received 20 January 2005; received in revised form 17 May 2005; accepted 8 June 2005
Available online 15 July 2005

Abstract

In this work, the complexation of cadmium and zinc ions by 3-[*N*-tris(hydroxymethyl)methylamine]-2-hydroxypropanesulfonic acid (TAPSO), a commercial biological buffer, was evaluated using three electrochemical techniques, at fixed total-ligand and total-metal concentration ratio and varied pH, at $25.0 \pm 0.1\,^{\circ}C$ and ionic strength set to 0.1 M KNO_3. For both metal–ligand systems, complexation was evidenced in the pH range close to deprotonation of the ligand and the final models were optimised after a meticulous graphical analysis.

For Cd–$(TAPSO)_x$–$(OH)_y$ system, two complexes, CdL and CdL_2, were identified in the buffering region of the ligand. The proposed final model for this system is: CdL, CdL_2 and $CdL_2(OH)$ with stability constants, as log β, of 2.2, 4.2 and 8.6, respectively.

For Zn–$(TAPSO)_x$–$(OH)_y$ system, the complex ZnL is the main species formed in the buffering pH range. The proposed final model is ZnL, ZnL(OH) and $ZnL(OH)_2$ with overall refined stability constants (as log β) to be: 2.5, 7.2 and 13.2, respectively.

Keywords: 3-[*N*-tris(Hydroxymethyl)methylamine]-2-hydroxypropanesulfonic acid; TAPSO; Biological buffer; Cadmium; Zinc; Stability constants

1. Introduction

The choice of alternative buffers had greatly increased with the commercial availability of the zwitterionic N-substituted aminosulfonic acids synthesized by Good and co-workers [1–3]. Good's buffers have, in fact, been widely adopted and at least one major chemical supplier devotes a special section of its catalogue to them (e.g., from Sigma–Aldrich).

In generating a series of more than 20 buffers for use in biological studies, these workers listed the prevention of metal ion complexation as one of their desired goals. However, most of a broad series of these buffers have been shown to cause metal ion interference as a result of complexation. Therefore, the knowledge of the stability constants of (Good buffer)–(metal ion) complexes is essential for accurate metal ions speciation studies in natural waters, biological fluids or industrial processes, when these biological buffers are required to be used.

As far as we know, no reports regarding studies of the interaction between TAPSO and cadmium are described in the literature. For zinc, there are some reports regarding studies of the ternary complexes of biological importance [4–6], but an exhaustive speciation study of Zn–$(TAPSO)_x$–$(OH)_y$ system has never been performed.

In previous studies, we have studied the interaction between 3-[*N*-tris(hydroxymethyl)methylamine]-2-hydroxypropanesulfonic acid (TAPSO) and copper [7] and

* Corresponding author. Tel.: +351 225081650; fax: +351 225081449.
E-mail addresses: cmachado@fe.up.pt (C.M.M. Machado), ignacy.cukrowski@up.ac.za (I. Cukrowski), hsoares@fe.up.pt (H.M.V.M. Soares).
[1] Tel.: +27 124202512; fax: +27 123625297.

0039-9140/$ – see front matter © 2005 Elsevier B.V. All rights reserved.
doi:10.1016/j.talanta.2005.06.003

lead [8]. These works evidenced that TAPSO forms several strong complexes with these metal ions in the pH buffer range, and thus, can decrease strongly the free metal ion concentration, when this ligand is used as a buffer. In this context, we think that the study of the interaction of TAPSO with cadmium and zinc may furnish a further contribution to obtain a systematic information of the overall stability constants of the (TAPSO)–(metal ion) systems where complexation occurs.

In the present study, the behaviour of solutions containing TAPSO and cadmium or zinc was studied by three electrochemical techniques: direct current polarography (DCP), differential pulse polarography (DPP) and GEP, at fixed total ligand to total metal concentration ($[L_T]$:$[M_T]$) ratios of various orders of magnitude and various pH values, at 25 °C and 0.1 M KNO_3 ionic strength. The final metal–ligand models for the two systems were obtained after a meticulous graphical analysis. The quasi-reversibility of the electrochemical reduction of zinc ion was fruitfully corrected with a simple procedure.

2. Experimental

2.1. Materials and reagents

For polarography, a stock solution of cadmium, 4.0×10^{-2} M, was prepared from the analytical grade salt ($Cd(NO_3)_2$, Merck) at pH 2.3 (addition of standardized nitric acid) and the ionic strength was adjusted to 0.1 M. For potentiometry, a Merck standard solution of cadmium (9.0×10^{-3} M) was used.

An acidic standard solution of zinc (1.5×10^{-2} M), purchased from Merck, was used for both techniques.

Additional information about the remaining reagents and experimental conditions were described previously [7].

2.2. Instrumentation

All measurements reported in this work were performed on solutions adjusted to ionic strength 0.1 M KNO_3 in a Metrohm (Herisau, Switzerland) jacketed glass vessel, equipped with a magnetic stirrer, and thermostated at 25.0 ± 0.1 °C using a water bath.

2.2.1. Polarography

The polarographic measurements of Cd–$(TAPSO)_x$–$(OH)_y$ system were performed using a computer controlled instrumental set-up [9] and a Model 663 VA stand (Metrohm) equipped with a multimode electrode (Metrohm, Model 6.1246.020), as a working electrode, used in the dropping mercury electrode mode. A silver/silver chloride (3 M KCl) electrode and a platinum electrode (both Metrohm) were used as reference and counter electrodes, respectively. In the DPP measurements, a pulse height of 50 mV was used, with a pulse width and an integration time of 200 and 60 ms, respectively. A drop time of 2 s and a step potential of 4 mV were used for both techniques (DC and DPP). The pH of cadmium solutions was measured to ±0.1 mV (±0.001 pH units) with a PHI 72 pH meter (Beckman) using a Model 6.0733.100 a silver/silver chloride, 3 M KCl reference and a Model 6.0133.100 glass electrodes, both from Metrohm.

Polarographic measurements of Zn–$(TAPSO)_x$–$(OH)_y$ system were performed using a Model 663 VA stand (Metrohm) equipped with a multimode electrode (Metrohm, Model 6.1246.020), as a working electrode, used in the dropping mercury electrode mode. A silver/silver chloride (3 M KCl) and a glassy carbon were used as reference and counter electrode, respectively (both from Metrohm). A drop time of 1 s and a step potential of 4 mV were used. For DPP mode, a modulation time of 20 ms and modulation amplitude of 50 mV were used. The VA stand was attached to a microAutolab system (Eco Chemie, Utrecht, The Netherlands) controlled by a personal computer. The pH measurements of the solutions were conducted with a GPL22 meter (Crison, Barcelona, Spain), with a sensitivity of ±0.1 mV (±0.001 pH units), with a silver/silver chloride reference electrode (Metrohm) and a glass electrode (Metrohm).

2.2.2. Potentiometry

Potentiometric titrations of Cd–$(TAPSO)_x$–$(OH)_y$ and Zn–$(TAPSO)_x$–$(OH)_y$ systems were performed with a PC-controlled system assembled with a Crison (Barcelona, Spain) MicroBU 2030 micro burette and a MicropH 2002 meter with a Philips GAH 110 glass electrode and an Orion 90-02-00 (Beverly, USA) double junction reference electrode with the outer chamber filled with background solution, 0.1 M KNO_3. Automatic acquisition of data was done by a home-made program, COPOTISY.

2.3. Procedure

For all techniques, the calibration of the glass electrodes (measurements of pH as $-\log_{10}[H^+]$), was achieved as previously described [7].

2.3.1. Direct current and differential pulse polarography

For both systems, Cd–$(TAPSO)_x$–$(OH)_y$ and Zn–$(TAPSO)_x$–$(OH)_y$, two polarographic techniques (DC and DP) were performed on the same sample solution. The procedure used to run the polarographic titrations was described elsewhere [7]; a set of 40 and 30 polarograms (representing all the species present at each pH value) were recorded for Cd–$(TAPSO)_x$–$(OH)_y$ and Zn–$(TAPSO)_x$–$(OH)_y$ systems, respectively. Several $[L_T]$:$[M_T]$ ratios were used for each system. For Cd–$(TAPSO)_x$–$(OH)_y$ system, two different $[L_T]$:$[Cd_T]$ ratios were evaluated, 186 and 308, with total cadmium concentration of 4.0×10^{-5} and 5.0×10^{-5} M, respectively. For Zn–$(TAPSO)_x$–$(OH)_y$ system, two $[L_T]$:$[Zn_T]$ ratios were evaluated, 150 and 255, with total zinc concentrations of 5.2×10^{-5} and 2.8×10^{-5} M, respectively.

The equilibrium of the metal–ligand solutions was tested and it was reached in a few minutes.

2.3.2. Glass electrode potentiometry

For Cd–$(TAPSO)_x$–$(OH)_y$ system, seven titrations, using three independent solutions, were performed in the pH range between 4.0 and 9.0. For each titration, about 50 points were collected and a $[L_T]$:$[Cd_T]$ ratio of 3.3 with a total cadmium concentration of 3.0×10^{-3} M was used.

For Zn–$(TAPSO)_x$–$(OH)_y$ system, five titrations, using two independent solutions, were carried out. For each titration, about 45 points were collected in the pH range between 3.0 and 7.5 and a $[L_T]$:$[Zn_T]$ ratio of 3.3 with a total zinc concentration of 7.6×10^{-4} M was used.

For both systems, monotonic additions of standardized KOH were done.

2.4. Data treatment

The simulation and optimisation procedures of potentiometric data was done using ESTA program [10,11]. The refinement operations used in potentiometry involve solving mass-balance equations, including equation for the total proton concentration, in such a way that the computed free proton concentration, when used by the equation describing the response of the calibrated glass electrode, reproduces the experimentally recorded potential of the glass electrode as accurately as possible.

The refinement of polarographic data was performed using the Cukrowski method, where all the equations that support theoretically the method are defined elsewhere [12,13]. This method uses mass-balance equations written for a labile (on the polarographic time scale) and reversible metal–ligand system studied at a fixed $[L_T]$:$[M_T]$ and varied pH. The refinement operations are based on the comparative analysis of the experimental and calculated complex formation curves, ECFC and CCFC, respectively.

During the refinement of the overall stability constants for both systems, the water [14] and ligand [7] protonation constants, as well as all known stability constants for $M_x(OH)_y$ species [14] (Table 1), were kept fixed.

3. Results and discussion

3.1. Ligand adsorption and metals reversibility studies

Ligand adsorption studies, reported in a previous paper [7], have shown that in the potential region where cadmium and zinc are reduced, no significant decrease of the capacitive current was observed in the concentration range studied ($[TAPSO] < 1.3 \times 10^{-2}$ M).

The polarograms recorded for Cd–$(TAPSO)_x$–$(OH)_y$ system indicated that the electrochemical process was fully reversible. For both polarographic titrations, fully reversible DC polarograms were recorded (gamma coefficient, which indicates the steepness of polarographic waves and whose theoretically value should be one for a reversible process, varied between 0.96 and 1.0) and DPP peak width, $w_{1/2}$, was constant throughout the experiment, 60.9 ± 0.1 mV (as predicted for a reversible process [15]).

Table 1
Dissociation constant for water, protonation constant for the ligand TAPSO and overall stability constants for Cd(II) and Zn(II) complexes with OH^-, at 25 °C

	Equilibrium	$\log \beta$	μ (M)	References
Water	$H^+ + OH^- \Leftrightarrow H_2O$	13.78	0.1	[14]
TAPSO	$L^- + H^+ \Leftrightarrow HL$	7.55	0.1	[7]
Cadmium	$Cd^{2+} + OH^- \Leftrightarrow Cd(OH)^+$	4.3	3.0	[14]
	$Cd^{2+} + 2OH^- \Leftrightarrow Cd(OH)_2$	7.7	3.0	[14]
	$Cd^{2+} + 3OH^- \Leftrightarrow Cd(OH)_3^-$	10.3	3.0	[14]
	$Cd^{2+} + 4OH^- \Leftrightarrow Cd(OH)_4^{2-}$	12.0	3.0	[14]
	$4Cd^{2+} + 4OH^- \Leftrightarrow Cd_4(OH)_4^{4+}$	24.9	3.0	[14]
	$Cd(OH)_2$ (s) $\Leftrightarrow Cd^{2+} + 2OH^-$	−14.29	3.0	[14]
Zinc	$Zn^{2+} + OH^- \Leftrightarrow Zn(OH)^+$	4.7	0.1	[14]
	$Zn^{2+} + 2OH^- \Leftrightarrow Zn(OH)_2$	10.2	0.0	[14]
	$Zn^{2+} + 3OH^- \Leftrightarrow Zn(OH)_3^-$	13.9	0.0	[14]
	$Zn^{2+} + 4OH^- \Leftrightarrow Zn(OH)_4^{2-}$	15.5	0.0	[14]
	$4Zn^{2+} + 4OH^- \Leftrightarrow Zn_4(OH)_4^{4+}$	27.9	3.0	[14]
	$Zn(OH)_2$ (s) $\Leftrightarrow Zn^{2+} + 2OH^-$	−14.82	0.1	[14]

For Zn–$(TAPSO)_x$–$(OH)_y$ system, the metal reduction process at the mercury electrode surface was not fully reversible. A decrease in the DC reversibility (decrease in the steepness of the polarographic wave from 0.94 to 0.65), in the pH range between 5.0 and 9.0, was observed. In Fig. 1, DCP waves of the metal zinc alone and of the metal in the presence of the ligand at pH values between pH 4.9 and 9.5 are plotted. As it is evidenced in figure, the irreversibility of the system increased strongly (wave steepness lowered down to below 0.4) for pH values above 9. In order to use the data for this system and since the limiting diffusion current I_d does not depend on the degree of reversibility of the electrochemical process, a correction for the departure from the reversibility of the recorded polarographic curves up to pH 9 was done. This procedure, described in a previous work [16], corrects the effect of the quasi-reversibility by fixing the gamma coefficient at value of 1 and computes the corrected limiting diffusion current and potential of half height, $E_{1/2}$, for electrochemically reversible process. For DPP and for ratio $[L_T]$:$[Zn_T] = 255$, the $w_{1/2}$ varied between 63.0 (metal alone) and 74.9 mV, with the increase of pH; a similar behaviour was obtained for $[L_T]$:$[Zn_T] = 150$. Attempts to correct DPP experimental curves, as described elsewhere [17], were not successful. Therefore, for Zn–$(TAPSO)_x$–$(OH)_y$ system, only DCP data were evaluated.

3.2. Modelling of Cd–$(TAPSO)_x$–$(OH)_y$ system and refinement of stability constants

The analysis of polarographic titrations (DC and DP polarography) data in a pH range between 5.0 and 9.5 using different $[L_T]$:$[Cd_T]$ ratios showed that Cd–$(TAPSO)_x$–$(OH)_y$ system behaved as labile and dynamic on the polarographic time scale; only one peak corresponding to all labile species present in solution, which shifted to more cathodic

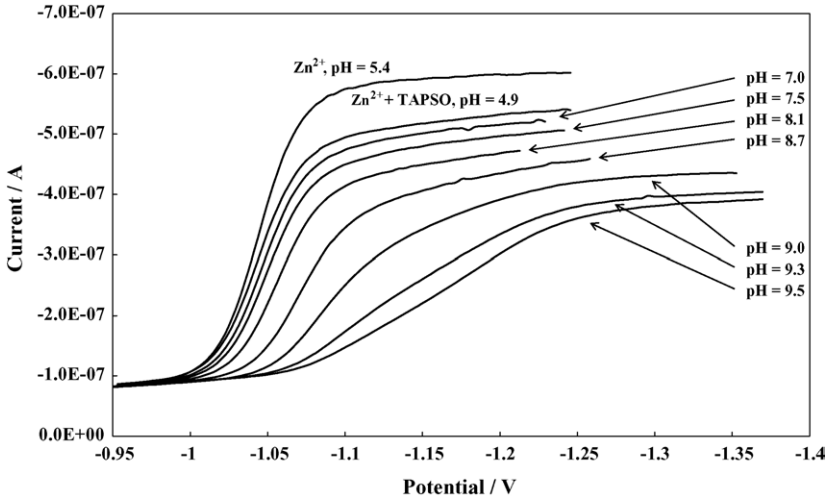

Fig. 1. Typical DC polarograms of zinc in the presence of TAPSO with the increase of pH. No correction for dilution was made (curves are seen as recorded).

potential values, was observed (data not shown). The analysis and discussion presented below is related to the DPP data.

The prediction of the metal–ligand species present in a solution was achieved by graphical analysis [13]; the plot of the peak potential as a function of the pH of the solution is presented in Fig. 2A. Protonation constant for the ligand and the different forms of the ligand (HL and L^-) according to the pH, are also marked in Fig. 2A. Four different regions were identified with the variation of pH. In the first region, up to pH 6.5, complexation was negligible; only 1.8 mV shift was observed. In region II, a slope of about 10 mV per pH unit was observed, which is smaller than one would expect for any metal containing species of a CdL type. Theoretical slope for CdL (one proton in the electrochemical reaction) would be (charges were omitted for sake of simplicity):

$$\mathrm{CdL} + \mathrm{H} + 2\mathrm{e} \Leftrightarrow \mathrm{Cd(Hg)} + \mathrm{HL}, \qquad \text{slope} = 30\,\mathrm{mV/pH}$$

But, between pH 6.5 and 8.5, the reaction with no proton involvement should also be considered:

$$\mathrm{CdL} + 2\mathrm{e} \Leftrightarrow \mathrm{Cd(Hg)} + \mathrm{L}, \qquad \text{slope} = 0\,\mathrm{mV/pH}$$

and this is probably the explanation why the slope has never developed to its theoretical value. So, CdL must be formed even though the slope did not suggest that. In region III, above pH 7.55, there was a decrease in the slope, followed by another drop in the slope around pH 8.2. For pH values higher than the pK_a, the ligand is mainly in the deprotonated form, which means that the main reduction reaction of CdL, at the DME, is the second reaction described above (no proton involved). This caused the decrease in the slope. The second drop must be due to the formation of other species. If only ML would be formed and present as a major metal containing species in the pH range between 8 and 9 then there should be no slope observed due to the fact that the ligand is almost entirely in its free form. The fact that the slope does not reach a value of zero (still small slope is observed between pH of 8.5 and 9) must indicate the formation of another species. The other species most likely would be CdL_2. It is important to emphasize that one must not expect the theoretical slope of about 59 mV/pH since we consider the data in the pH range where ligand is almost fully deprotonated. Moreover, the formation of OH containing species below pH 9 would make the slope much more pronounced. For instance, the formation of Cd(OH) and/or $CdL_x(OH)$, would increase the slope significantly, since the reduction at the DME electrode generates a slope of about 30 mV according to the following reaction:

$$\mathrm{CdL}_x\mathrm{(OH)} + \mathrm{H} + 2\mathrm{e} \Leftrightarrow \mathrm{Cd(Hg)} + x\mathrm{L} + \mathrm{H_2O},$$

$$\text{slope} = 30\,\mathrm{mV/pH}$$

The final increase in the slope, above pH of 9.0, clearly indicated the formation of $CdL_x(OH)$ species (region IV).

The analysis of the observed peak potential versus log [L] (Fig. 2B) confirmed the formation of CdL (the slope reached a value of about 30 mV per log unit) in the pH range between 7.4 and 8.4. Assuming the formation of CdL_2, one would not observe the theoretically expected slope of about 59 mV/log [L] because this complex is formed in the pH range where there is no further increase in the free ligand concentration (see last points that aim at a fixed value of the free ligand concentration).

In Fig. 2C, the variation of the peak height with pH is represented. The smooth drop in the peak height indicates the formation of complexed species between the metal and the ligand. A careful analysis of the normalized peak height corroborated the formation of the species mentioned above. The normalized current started to decrease around pH 6.5, where complexation started, as it is evidenced in Fig. 2A. At pH 7.5, the normalized peak height had a total drop of about 0.1 units due to the formation of CdL. Then, the normalized peak height continues to decrease gradually. At pH ≈ 8.2, the observed drop in the normalized peak height is explained by the beginning of formation of CdL_2. Around pH 9, the

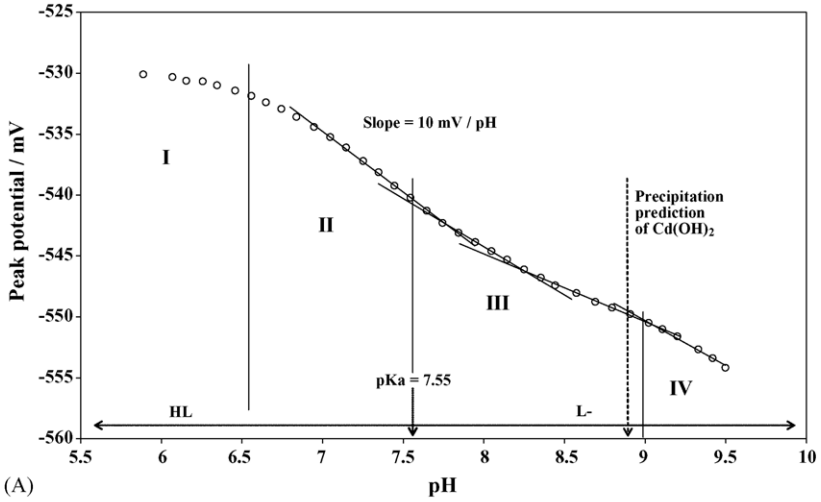

(A)

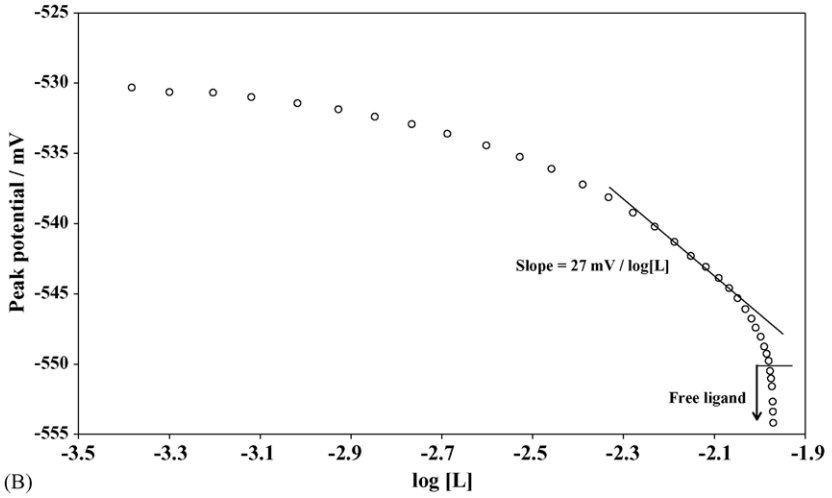

(B)

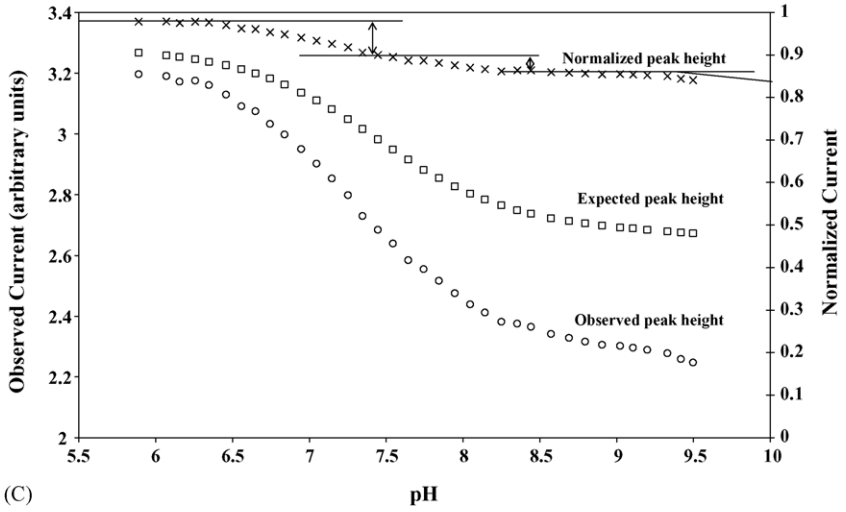

(C)

Fig. 2. Graphic analysis of the data obtained for the Cd–$(TAPSO)_x$–$(OH)_y$ system by DPP. (A) E_p vs. pH; (B) E_p vs. log [L]; (C) I_p vs. pH. $[L_T]:[Cd_T] = 308$, $[Cd^{2+}] = 5.0 \times 10^{-5}$ M.

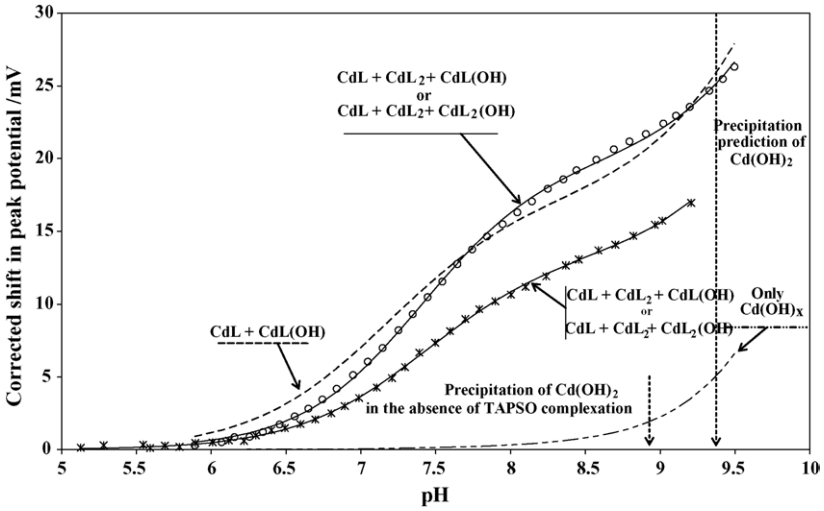

Fig. 3. Modelling of the Cd–$(TAPSO)_x$–$(OH)_y$ system by use of complex formation curves. Circles and asterisks represent the experimental complex formation curves for $[L_T]:[Cd_T] = 308$, $[Cd^{2+}] = 5.0 \times 10^{-5}$ M and $[L_T]:[Cd_T] = 186$, $[Cd^{2+}] = 4.0 \times 10^{-5}$ M, respectively. The fitted models are indicated in the figure (CCFC are seen as solid lines) and the refined stability constants are summarized in Table 2.

hydroxide species starts to be formed and this explains further small drop in the normalized peak height.

From the graphical analysis described above, the Cd–$(TAPSO)_x$–$(OH)_y$ model should include CdL, CdL_2 and $CdL_x(OH)$ species.

In Fig. 3, the ECFC for $[L_T]:[Cd_T] = 308$ (open circles) and $[L_T]:[Cd_T] = 186$ (asterisks), as well as the CCFC for $Cd_x(OH)_y$ species, are included. The comparison of the CCFC for $Cd_x(OH)_y$ (– - –) with both ECFC clearly evidences complexation between TAPSO and cadmium. At pH 8.0, if no complexation with TAPSO occured, the shift of the potential should be zero, as it is evidenced by the CCFC for $Cd_x(OH)_y$ species, but a shift of 10 mV was observed, for the lowest ratio. In addition, precipitation of $Cd(OH)_2$, in the absence of TAPSO complexation, was predicted around pH 8.9 and this was not confirmed experimentally. In conclusion, these facts evidence that it was not possible to make such a large experimental error and clearly confirms that TAPSO forms complexes with cadmium. In addition, it is also observed that the CCFC for $Cd_x(OH)_y$ species is parallel to both ECFC at highest pH values. This indicates that the metal hydroxide species, $Cd_x(OH)_y$, and the $CdL_x(OH)_y$ species are formed in the same pH region.

Next, a special procedure that was based on simulation of CCFC assuming several models and comparing them with the ECFC curves was used to propose the final model (Fig. 3). The strategy used is summarized in Table 2.

Even though the graphic analysis in Fig. 2 has suggested that CdL_2 would probably be present in the solution (Fig. 2A and C), we decided to test a simpler model by fitting CdL with CdL(OH) into the experimental data (Model I in Table 2 and Fig. 3). However, when the stability constants for these two species were refined, it became obvious that more species must be formed. Statistically, the refined CdL + CdL(OH) model had an excellent standard deviation for both ratios, namely for the lower one. However, the graphical analysis of the fitting revealed that this model was not the correct one, as it is exemplified for the highest ratio in Fig. 2. The CCFC for

Table 2
Overall stability constants (as $\log\beta$ values) for Cd–$(TAPSO)_x$–$(OH)_y$ system determined at 25 °C and $\mu = 0.1$ M by DPP for $[L_T]:[Cd_T] = 186$, $[Cd^{2+}] = 4.0 \times 10^{-5}$ M (38 points, between pH 5.1 and 9.2) and for $[L_T]:[Cd_T] = 308$, $[Cd^{2+}] = 5.0 \times 10^{-5}$ M (36 points, between pH 5.9 and 9.5) and by GEP for $[L_T]:[Cd_T] = 3.3$, $[Cd^{2+}] = 3.0 \times 10^{-3}$ M (88 points, two titrations, from pH 4.0 to 8.0)

Complexes	Equilibrium	DPP $[L_T]:[Cd_T] = 186$			DPP $[L_T]:[Cd_T] = 308$			GEP $[L_T]:[Cd_T] = 3.3$
		Model I	Model II	Model III	Model I	Model II	Model III	
CdL^+	$Cd^{2+} + L^- \Leftrightarrow CdL^+$	2.41 ± 0.02	2.30 ± 0.07	2.30 ± 0.07	2.42 ± 0.01	2.14 ± 0.07	2.14 ± 0.07	2.31 ± 0.02
CdL_2	$Cd^{2+} + 2L^- \Leftrightarrow CdL_2$	NI	4.2 ± 0.2	4.2 ± 0.2	NI	4.27 ± 0.07	4.28 ± 0.07	4.40 ± 0.03
CdL(OH)	$Cd^{2+} + L^- + OH^- \Leftrightarrow CdL(OH)$	6.7 ± 0.1	6.4 ± 0.3	NI	6.83 ± 0.04	6.59 ± 0.09	NI	NI
$CdL_2(OH)^-$	$Cd^{2+} + 2L^- + OH^- \Leftrightarrow CdL_2(OH)^-$	NI	NI	8.6 ± 0.3	NI	NI	8.55 ± 0.09	R
SD (mV)		0.107	0.013	0.013	1.1701	0.0418	0.0415	
Hamilton *R*-factor								0.027

For DPP, SD represents an overall fit of complex formation curves, the computed curve in the objective experimental function [7]. For GEP, Hamilton *R*-factor stands for a statistical Hamilton *R*-factor generated by the program ESTA [11]. NI, not included; R, rejected.

this model (dashed line in Fig. 3) had two cross-points, at pH 7.7 and 9.2. Between pH 6.0 and 7.7, the CCFC was above the experimental data (ECFC); this means that the computed stability constant for CdL, the main specie present in solution in this pH range, was too large; log K_1 must be smaller than 2.4. Between pH 7.7 and 9.2, the CCFC was bellow the ECFC; this fact indicated that even though log K_1 was too large, the complex CdL could not make the observed shift difference, suggesting that another species, not containing the OH group, was missing in the metal–ligand model. Above pH 9.2, the CCFC was above the ECFC, which indicates that the calculated log $\beta_{CdL(OH)}$ was too large.

In the next step, we included CdL_2 in the model (Table 2, Model II), as it was suggested from the graphical analysis of Fig. 2 and discussion above related to CCFC for the model containing CdL and CdL(OH). This resulted in a very good fitting with a low overall standard deviation for both $[L_T]$:$[Cd_T]$ ratios. If one assumes that CdL(OH) should be a product of hydrolysis of the complex CdL, then the value of the refined stability constant for CdL(OH) was almost as expected from hydrolysis ($\log \beta_{CdL(OH)} = \log \beta_{CdL} + \log \beta_{Cd(OH)} = 2.3 + 4.3 = 6.6$).

If one accepts the strategy the simpler model the better, when refinement of data is concerned, then the model CdL, CdL_2 and CdL(OH) could be accepted. On the other hand, one might assume that the hydrolysis of CdL_2 may also take place. Hence, it was decided to incorporate this complex in the model; the refinement operations of the data, for which CdL, CdL_2 and CdL_2(OH) were included in the model (Table 2, Model III) gave a similar fitting as that obtained for model II (Fig. 3, solid line). These facts showed that, as expected, it was not possible to distinguish between CdL(OH) and CdL_2(OH); note that these complexes are formed exactly in the same pH range where the ligand is fully deprotonated, and the same slope is obtained, both complexes require the same amount of protons:

$$CdL_x(OH) + H + 2e \Leftrightarrow Cd(Hg) + xL + H_2O$$

From the above it follows that two complexes, namely CdL, and CdL_2, were identified with high certainty and their stability constants did not vary much when different hydroxo complexes $CdL_x(OH)_y$ were incorporated in the metal–ligand model. In addition, the complexes CdL and CdL_2 are most important when buffering pH range of the ligand TAPSO is of interest. It is impossible, for reason given above, to distinguish between CdL(OH) and CdL_2(OH), regardless of analytical technique used as these complexes are formed where there is not a protonated form of the ligand present; an increase in pH does not change the free ligand concentration. These two complexes, CdL(OH) and CdL_2(OH), describe the system equally well and since they are formed outside the buffering pH range, they are not of importance in this type of the study.

Modelling of the solution composition for potentiometric analytical conditions (using the models and stability constants obtained from polarography) suggested that it should be possible to establish CdL and CdL_2 stability constants prior to precipitation. It was also predicted that no information about $CdL_x(OH)_y$ species would be available from the GEP experiments (data not shown). Based on the polarographic results and predictions made for the best analytical conditions, GEP experiments were performed. Precipitation was observed at pH 8.0. The refined results for data collected between pH 4.0 and 8.0 from two titrations are summarized in Table 2. Similar results were obtained with the other titrations. When the model CdL, CdL_2 and CdL_2(OH) was investigated then the complex CdL_2(OH) was always rejected in the refinement operations or resulted in unreasonable stability constant values. The stability constant values obtained for CdL and CdL_2 were very comparable with the ones obtained by DPP, being the differences within the experimental errors.

Taking into account the different ratios and the different techniques performed, the following values for the stability constants (as log β values) are proposed for the complexes formed in the buffering pH region: CdL = 2.2 ± 0.2, CdL_2 = 4.2 ± 0.2, and for most likely hydroxo species, CdL(OH) = 6.4 ± 0.2 and CdL_2(OH) = 8.6 ± 0.2 (note that the standard deviations indicate here the ranges in stability constants obtained from different ratios and techniques and are within the experimental errors associated with both techniques).

Species distribution diagrams for model CdL, CdL_2 and CdL_2(OH), for $[L_T]$:$[Cd_T]$ = 308 and for $[L_T]$:$[Cd_T]$ = 3.3 were plotted in Fig. 4. This figure shows that CdL and CdL_2 are the major species in solution in the buffering pH range (between pH 6.5 and 8.5) (a similar behaviour was obtained for $[L_T]$:$[Cd_T]$ = 186, data not shown); only 37% of CdL_2(OH) was predicted at pH 9.5, the highest pH for which experimental points were collected for $[L_T]$:$[Cd_T]$ = 308 in DPP experiments. Fig. 4 also evidences that, for GEP experimental conditions, no significant amount of CdL_2(OH) was formed up to pH 8.0, which explains why this species was rejected in the GEP refinement operations. For model CdL, CdL_2 and CdL(OH), similar species distribution diagrams were drawn, resulting in the same conclusions (data not shown).

The comparison of the values of the stability constants determined for Cd–$(TAPSO)_x$–$(OH)_y$ in this work with other β-alcohols–amino ligands reported in the literature (triethanolamine, 2-amino-1-propanol, 2-amino-1-butanol, 2-amino-1-pentanol, 2-amino-1,3-propanediol)-[14,18]evidenced that the stability constants for CdL and CdL_2 are of the same order of magnitude.

3.3. Modelling of Zn–$(TAPSO)_x$–$(OH)_y$ system and refinement of stability constants

Fig. 1 evidences that Zn–$(TAPSO)_x$–$(OH)_y$ system behaves as fully labile, since only one DC wave was registered in the pH range studied, corresponding to all the species present in solution.

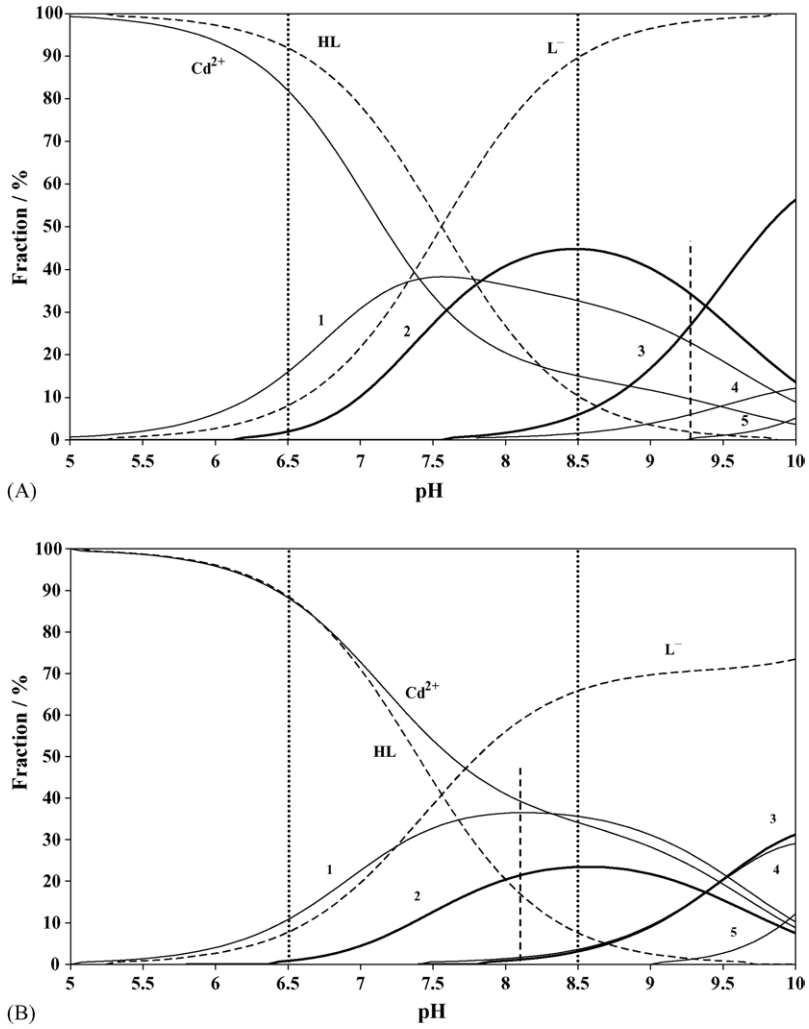

Fig. 4. Species distribution diagrams computed for (A) $[L_T]$:$[Cd_T] = 308$, $[Cd^{2+}] = 5.0 \times 10^{-5}$ M and (B) $[L_T]$:$[Cd_T] = 3.3$, $[Cd^{2+}] = 3.0 \times 10^{-3}$ M. The Cd–$(TAPSO)_x$–$(OH)_y$ model used was: CdL (1), CdL_2 (2) and $CdL_2(OH)$ (3), for which stability constant values, as $\log \beta$, were 2.2, 4.2 and 8.6, respectively. $Cd_x(OH)_y$ species were also considered (Table 1): Cd(OH) (4), $Cd(OH)_2$ (5). Dashed line represents $Cd(OH)_2$ precipitation and the pH range bounded by the dotted lines indicates the pH buffering region.

After the correction of the waves regarding reversibility[16], the corrected half-wave potential as a function of pH was plotted (Fig. 5). The different forms of the ligand according to the pH range and TAPSO's pK_a value were also marked in Fig. 5. The function shows a continuous and rather small shift of the half-wave potential towards cathodic potentials. Note that the total shift was around 45 mV. A slope of about 44 mV/pH, between pH 8.5 and 9.0, was the only one, which was possible to identify. This slope suggests the presence in solution of $ZnL_x(OH)_y$ species. Reaction at the DME electrode with two protons involved should develop a slope of 59 mV/pH unit (charges omitted for sake of simplicity):

$$ZnL_x(OH)_2 + 2H + 2e \Leftrightarrow Zn(Hg) + xL + 2H_2O,$$

$$\text{slope} = 59\,\text{mV/pH}$$

The fact that the slope did not develop to its theoretical value indicates the presence of some amount of $ZnL_x(OH)$ (one proton implicated):

$$ZnL_x(OH) + H + 2e \Leftrightarrow Zn(Hg) + xL + H_2O,$$

$$\text{slope} = 30\,\text{mV/pH}$$

and most likely still the reduction of the complex ZnL (no proton involved):

$$ZnL + 2e \Leftrightarrow Zn(Hg) + L, \qquad \text{slope} = 0\,\text{mV/pH}$$

causing the observed slope having a resultant value of several electrochemical processes taking place at the working electrode simultaneously.

The analysis of the variation of the observed half-wave potential with the concentration of free ligand (insert in Fig. 5), which should allow us to predict ZnL_n species, does not indicate in an obvious way the complexation between zinc and TAPSO (there is not a slope of about 30 mV/log [L] as expected for ZnL).

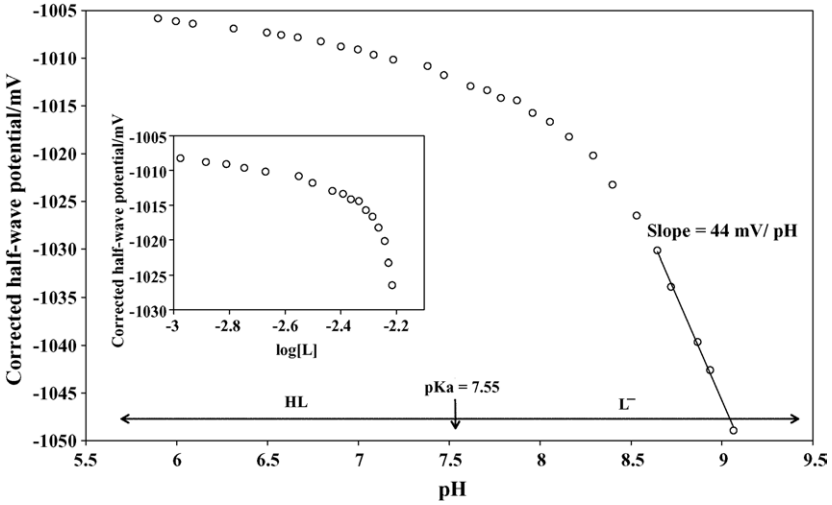

Fig. 5. Corrected half-wave potential as a function of pH and as a function of the free ligand concentration (insert in this figure) obtained by DCP for Zn–(TAPSO)$_x$–(OH)$_y$ system. [L_T]:[Zn_T] = 255, [Zn^{2+}] = 2.8×10^{-5} M.

It is very important to emphasize that complexation occurs in the pH range, where the ligand is being deprotonated, becoming the main form of the ligand present in solution (Fig. 5). This means that the slope analysis is difficult, since no theoretical slope will appear in the region where the deprotonation occurs considering the absence of hydroxide species ($ZnL_x + 2e \Leftrightarrow Zn(Hg) + xL$, slope = 0 mV/pH). Note that up to pK_a 7.55, only 8.6 mV shift was observed, indicating that the highest amount of complexed species should exist at pH values higher than the pK_a. A similar behaviour was observed for Cd–(TAPSO)$_x$–(OH)$_y$ system (Fig. 2A). Note that for both systems, the ML complex starts to be formed in the deprotonation pH range, indicating that the highest amount of complexed species exist after the pK_a, which complicates the system characterization.

From the analysis of data seen in Fig. 5 one could conclude that the species $ZnL_x(OH)_y$ were detected and ZnL was expected to be formed to some extent. Assuming simplest model one should consider ZnL, ZnL(OH) and $ZnL(OH)_2$.

Next, several calculated complex formation curves were generated to help in the decision on the final model of this system (Fig. 6). The CCFC for only $Zn_x(OH)_y$ species (dashed line curve) evidenced a lower shift than the ECFC. This was an unequivocal indication of complexation, even though the difference between the two curves at pH 8.0 (where the metal hydroxides species start to form) was only about 12 mV. Similar to what was observed with Cd–(TAPSO)$_x$–(OH)$_y$ system, the CCFC for metal–hydroxide species was parallel to the ECFC (open circles in Fig. 6 at highest pH values), which means that $ZnL_x(OH)_y$ and $Zn(OH)_y$ species exist in the same pH range. When we compare the CCFC (dotted line curve) calculated only for hydroxide species (ZnL(OH), $ZnL(OH)_2$ and $Zn_x(OH)_y$) with the experimental data (circles), this clearly shows that this model does not describe the system. From pH 6.0 to 8.0, the CCFC is below the ECFC,

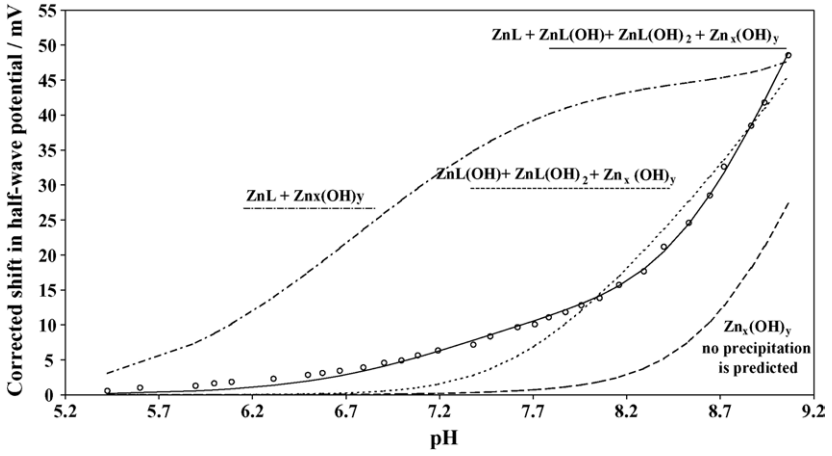

Fig. 6. Experimental (points, DCP data) and calculated (lines) complex formation curves for the Zn–(TAPSO)$_x$–(OH)$_y$ system. [L_T]:[Zn_T] ratio 255, [Zn^{2+}] = 2.8×10^{-5} M. The stability constant values are shown in Table 3.

Table 3
Overall stability constants (as $\log\beta$ values) for Zn–$(TAPSO)_x$–$(OH)_y$ system, determined at 25 °C and $\mu = 0.1$ M by DCP for $[L_T]:[Zn_T] = 150$, $[Zn^{2+}] = 5.2 \times 10^{-5}$ M (26 points, from pH 4.9 to 9.0) and for $[L_T]:[Zn_T] = 255$, $[Zn^{2+}] = 2.8 \times 10^{-5}$ M (30 points, between pH 5.4 and 9.1) and by GEP for $[L_T]:[Zn_T] = 3.3$, $[Zn^{2+}] = 7.6 \times 10^{-4}$ M (two titrations, 84 points, between pH 4.5 and 7.7)

Complexes	Equilibrium	DCP $[L_T]:[Zn_T] = 255$		DCP $[L_T]:[Zn_T] = 150$		GEP $[L_T]:[Zn_T] = 3.3$
		Model I	Model II	Model I	Model II	
ZnL^+	$Zn^{2+} + L^- \Leftrightarrow ZnL^+$	NI	2.45 ± 0.03	NI	2.47 ± 0.03	2.63 ± 0.02*
ZnL(OH)	$Zn^{2+} + L^- + OH^- \Leftrightarrow ZnL(OH)$	8.29 ± 0.02	7.2 ± 0.4	8.30 ± 0.02	7.2 ± 0.4	NI
$ZnL(OH)_2^-$	$Zn^{2+} + L^- + 2OH^- \Leftrightarrow ZnL(OH)_2^-$	12.0 ± 0.5	13.14 ± 0.05	12.95 ± 0.06	13.27 ± 0.03	NI
SD (mV)		8.7	0.29	10.2	0.75	
Hamilton *R*-factor						0.030

For DCP, SD represents an overall fit of complex formation curves, the computed curve in the objective experimental function [7]. For GEP, Hamilton *R*-factor stands for a statistical Hamilton *R*-factor generated by the program ESTA [11]. NI, not Included
* Simultaneous refinement of acid concentration with a maximum variation of 1.7%.

which suggests the formation of another species prior to the formation of hydroxo species; clearly, the complex ZnL must be included. Above pH 8.0 the inclusion of only hydroxide species in the M–L model makes the CCFC approaching the ECFC, but still does not describe totally the experimental data. The refined stability constants are summarized in Table 3. The refined value for ZnL(OH) stability constant is very high when the complex ZnL is not included in the

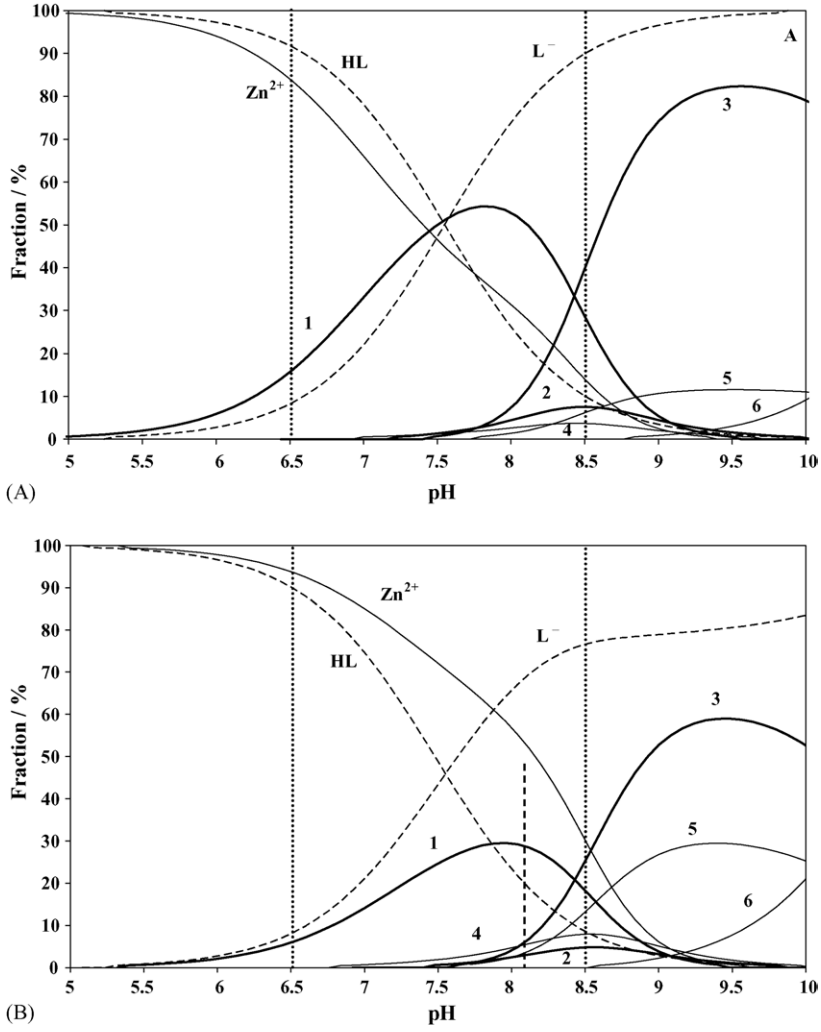

Fig. 7. Species distribution diagrams for the Zn–$(TAPSO)_x$–$(OH)_y$ system. (A) $[L_T]:[Zn_T]$ ratio 255, $[Zn^{2+}] = 2.8 \times 10^{-5}$ M; (B) $[L_T]:[Zn_T] = 3.3$, $[Zn^{2+}] = 7.6 \times 10^{-4}$ M. Stability constants were set to (as $\log\beta$ values): ZnL = 2.5 (1), ZnL(OH) = 7.2 (2) and $ZnL(OH)_2$ = 13.2 (3). $Zn_x(OH)_y$ species were also considered (Table 1): Zn(OH) (4), $Zn(OH)_2$ (5) and $Zn(OH)_3$ (6). Dashed line represents $Zn(OH)_2$ precipitation and the pH range bounded by the dotted lines indicates the pH buffering region.

M–L model; if one considers the hydrolyses of the ZnL complex, $\log \beta_{ZnL} + \log \beta_{Zn(OH)} = \log \beta_{ZnL(OH)}$, this would result with a value for $\log \beta_{ZnL}$ of 3.5. This value is too high for Zn–TAPSO complexation. For the same ligand, we should expect that Pb(II) forms stronger complexes with TAPSO than zinc [14], but the computed value was of the same order of magnitude [8]. The refined stability constant for $ZnL(OH)_2$ was close to the theoretically expected value. In addition, the overall fit was rather large, indicating that this model was not correct. In the next step, we decided to include the ZnL complex in the model (Table 3, Model II and Fig. 6), as some indication of its presence was suggested in Fig. 5 and since this was the only reasonable complex to be considered here. This improved significantly the overall fit (Table 3, Model II) and the CCFC fitted very well the experimental points (solid line in Fig. 6).

For triethanolamine, stability constants for ZnL and ZnL_2 are reported in the literature [14]. However, for $Zn–(TAPSO)_x–(OH)_y$ system, no experimental evidence of the presence of ZnL_2 was observed (Fig. 5). When the model containing ZnL, ZnL_2 and $ZnL(OH)_2$ was allowed to be refined, the complex ZnL_2 was systematically rejected (data not shown).

Using the stability constant values refined from DCP experiments, a glass electrode potentiometry experiment was designed. Due to the early precipitation, around pH 7.8, only stability constant for ZnL was possible to refine (Table 3). This system showed to be very sensitive to the acid concentration and simultaneous refinement of this parameter had to be done in order to obtain reasonable results. Only the results, for which the variation of this parameter were lower than 2% were used. The refined results for data collected between pH 4.5 and 7.7 from two titrations are summarized in Table 3. Similar results were obtained with the other titrations.

Considering potentiometric and polarographic experiments, the final model for $Zn–(TAPSO)_x–(OH)_y$ system is: ZnL, ZnL(OH) and $ZnL(OH)_2$, with stability constants set to (as $\log \beta$ values): 2.5 ± 0.1, 7.2 ± 0.4 and 13.2 ± 0.1, respectively. Using these values, species distribution diagrams for $[L_T]:[Zn_T]$ ratios 255 and 3.3 were plotted (Fig. 7). Observing the diagrams, it is clear why the stability constant value for ZnL(OH) has a large standard deviation, it exists in a very small amount for both ratios (Fig. 7). For $[L_T]:[Zn_T]$ ratio 255, at pH 8.5, where ZnL(OH) exists in higher amount, there is only 8% of ZnL(OH), while 29% of ZnL and 40% of $ZnL(OH)_2$ are predicted in solution (Fig. 7A). Therefore, it is understandable that the standard deviation associated with this constant would be large and for evident reasons, this species practically does not influence the system characterization. ZnL and $ZnL(OH)_2$ complexes are the most important species, which will influence the free zinc ion in the buffering pH region. Now, the absence of slopes in the polarographic graphical analysis (Fig. 5) is also clear. ZnL is formed exactly in the deprotonation region, and even though 53% exists at $pH = pK_a$ (Fig. 7A), the observed shift was only 8.6 mV (Fig. 5). Fig. 7B also evidences that, for GEP experimental conditions, ZnL was the only specie formed before precipitation was predicted and this was just what was observed experimentally (precipitation was detected around pH 7.8) (Fig. 7B).

When we compare the final models obtained for $Cd–(TAPSO)_x–(OH)_y$ and $Zn–(TAPSO)_x–(OH)_y$ systems, the main difference is that, for $Cd–(TAPSO)_x–(OH)_y$ system, a large amount of CdL_2 is formed in a wide range of pH (between pH 7.5 and 9.0) for higher $[L_T]:[Cd_T]$ ratios, whereas for $Zn–(TAPSO)_x–(OH)_y$ system in the same pH range, no experimental evidence of ZnL_2 was detected and ZnL is the main specie followed by an exponential increase of $ZnL(OH)_2$. This fact can be easily understood. First, the stability constant of ZnL is slightly higher than the stability constant determined for CdL. In addition, the stability constant value for $Zn(OH)_2$ is more than two orders of magnitude larger than that for $Cd(OH)_2$ (Table 1), which favours the formation of $ZnL(OH)_2$ instead of ZnL_2.

Literature describes stability constants for ZnL of the same order of magnitude for other similar β-alcohols–amino ligands (2.27 and 2.38 for 2-amino-2-hydroxymethyl-1,3-propanediol (THAM or TRIS) and 2-bis(2-hydroxyethyl)amino-2-hydroxymethyl-1,3-propanediol (BIS–TRIS), respectively) [14]. On the other hand, some recent studies [4–6] have described stability constants values for ZnL ($\log \beta$ between 3.60 and 3.80) significantly different from the value obtained in this work. It has been decided to generate the CCFC for this model, ZnL plus $Zn_x(OH)_y$ species, as reported in the literature (an average value of all published values for $\log \beta_{ZnL}$ was used, $\log \beta_{ZnL} = 3.70$, see line (- · -) in Fig. 6).The CCFC clearly shows that the value of stability constant is too high and does not describe the experimental values (ECFC).

Acknowledgements

The authors thank the "Fundação para a Ciência e a Tecnologia" from Portuguese Government for the financial support of this work with FEDER funds, by the project POCTI/39950/QUI/2001. We also thank Professor Carlos Gomes from the Faculty of Sciences/Porto University for the COPOTISY program.

References

[1] N.E. Good, G.D. Winget, W. Winter, T.N. Connolly, S. Izawa, R.M.M. Singh, Biochemistry 5 (1966) 467.
[2] N.E. Good, S. Izawa, Methods Enzymol. B 29 (1972) 53.
[3] W.J. Ferguson, K.I. Braunschweiger, W.R. Braunschweiger, J.R. Smith, J.J. McCormick, C.C. Wasmann, N.P. Jarvis, D.H. Bell, N.E. Good, Anal. Biochem. 104 (1980) 300.
[4] Z.M. Anwar, H.A. Azab, J. Chem. Eng. Data 44 (1999) 1151.
[5] H.A. Azab, F.S. Deghaidy, A.S. Orabi, N.Y. Farid, J. Chem. Eng. Data 45 (2000) 709.

[6] Z.M. Anwar, H.A. Azab, J. Chem. Eng. Data 46 (2001) 34.
[7] C.M.M. Machado, I. Cukrowski, P. Gameiro, H.M.V.M. Soares, Anal. Chim. Acta 493 (2003) 105.
[8] C.M.M. Machado, I. Cukrowski, H.M.V.M. Soares, Electroanalysis (2005), in press.
[9] I. Cukrowski, E. Cukrowska, R.D. Hancock, G. Anderegg, Anal. Chim. Acta 312 (1995) 307.
[10] P.M. May, K. Murray, D.R. Williams, Talanta 32 (1985) 483.
[11] P.M. May, K. Murray, D.R. Williams, Talanta 35 (1988) 825.
[12] I. Cukrowski, Anal. Chim. Acta 336 (1996) 23.
[13] I. Cukrowski, M. Adsetts, J. Electroanal. Chem. 429 (1997) 129.
[14] R.M. Smith, A.E. Martell, NIST Standard Reference Database 46. NIST Critically Selected Stability Constants of Metal Complexes Database, Version 3.0, US Department of Commerce, National Institute of Standards and Technology, 1997.
[15] E.P. Parry, R.A. Osteryoung, Anal. Chem. 37 (1965) 1634.
[16] C.M.M. Machado, I. Cukrowski, H.M.V.M. Soares, Helv. Chim. Acta 86 (2003) 3288.
[17] I. Cukrowski, S.A. Loader, Electroanalysis 10 (1998) 877.
[18] S. Canepari, C. Vincenzo, P. Castellano, A. Messina, Talanta 47 (1998) 1077.